

# All-Inorganic Perovskite Solar Cells: Modification Strategies and Challenges

Xin-Yi Li, Qi Sun, Yue-Min Xie,\* and Man-Keung Fung\*

Cesium-based all-inorganic wide-bandgap perovskite solar cells (AIWPSCs) have been demonstrated with exceptional optoelectronic properties such as intrinsic optical wide-bandgap and high thermal stability, which make them suitable candidates for the front sub-cells of tandem solar cells (TSCs). Passivation of perovskite surface and interface is a matter of common interest in this community since all-inorganic perovskites always suffer from non-ideal crystallization such as phase impurity, high defect density, and non-uniform morphology. Despite these shortcomings, numerous efforts have been devoted in recent years to pursuing high-performance AIWPSCs, which exhibit an abruptly increased power conversion efficiency (PCE) from 2.9% to over 21.0%. In view of not having a thorough summary about the advancements on AIWPSCs, herein, a comprehensive review is given to highlight the recent device performance progress of AIWPSC, particularly focusing on the strategies to passivate the defects of all-inorganic perovskite, namely, additive engineering, solvent engineering, interface modification, and the exploration of new charge transport materials (CTMs) for improving the phase stability and PCE of AIWPSCs. Finally, a conclusive outlook on AIWPSCs will be given to provide our perspectives aiming to inspire the further development of AIWPSCs.

## 1. Introduction

Numerous advantages such as high power conversion efficiency (PCE),<sup>[1]</sup> low production cost,<sup>[2,3]</sup> flexibility in form factor,<sup>[4,5]</sup> and compatibility with tandem devices,<sup>[6]</sup> have propelled perovskite solar cells (PSCs) to become the star among a number of photovoltaic materials.<sup>[7–9]</sup> Encouragingly, after approximately 10 years of development, the PCE of single-junction PSCs has been boosted from 3.8% in 2009 to an impressive 26.1% in 2023.<sup>[10–12]</sup> In particular, compared with single-junction PSCs, wide-bandgap perovskite sub-cells (WPSCs)-based monolithic tandem solar cells (TSCs) are distinguished with high open-circuit voltage ( $V_{OC}$ ) and the capability to surpass the Shockley–Queisser limit, which has achieved high PCE values over 33%,<sup>[13]</sup> illustrating promising commercialization prospects.

Typically, perovskite-based monolithic TSCs can be classified into four types, namely, perovskite/perovskite,<sup>[14–16]</sup> perovskite/organic,<sup>[17]</sup> perovskite/silicon, and perovskite/CIGS TSCs.<sup>[18]</sup> For AIWPSCs-based two-junction TSCs, Chen et al. reported the first two-junction TSCs by integrating AIWPSCs with organic solar cells.<sup>[19]</sup> However, limited by the compromised efficiency of the sub-cells, the tandem device efficiency is merely 14.03%. After that, Liu et al. reported AIWPSCs-based all-perovskite two-junction TSCs, and a PCE of 27.4% was obtained.<sup>[20]</sup> Moreover, they also reported AIWPSCs-based 4-T triple-junction tandem solar cells by sequentially depositing organic-inorganic perovskite-based medium bandgap sub-cells and silicon-based small bandgap sub-cells on the AIWPSCs. These triple-junction tandem solar cells facilitate a high PCE of 35.35%, which illustrates the potential of triple-junction devices to enhance the PCE of the devices. Moreover, Wang et al. fabricated high-efficiency AIWPSCs for all perovskite triple-junction TSCs with a PCE of 24.3%, which indicates the great potential of triple-junction TSCs in achieving high-efficiency devices.<sup>[21]</sup>

Regardless of the specific type of tandem solar cells, WPSCs are inevitable, and the photoelectric properties of WPSCs have a profound impact on the photovoltaic performance of their integrated tandem devices. In general, with respect to the A-site cation composition in the perovskite chemical structure (ABX<sub>3</sub>), WPSCs can be categorized into two main types, namely, organic cation-based organic-inorganic mixed-halide wide-bandgap

---

X.-Y. Li, Q. Sun, Y.-M. Xie, M.-K. Fung  
Institute of Functional Nano & Soft Materials (FUNSOM)  
Jiangsu Key Laboratory for Carbon-Based Functional Materials & Devices  
Soochow University  
Suzhou, Jiangsu 215123, P. R. China  
E-mail: ymxie@suda.edu.cn; m kfung@suda.edu.cn

Q. Sun, M.-K. Fung  
Macao Institute of Materials Science and Engineering (MIMSE)  
MUST-SUDA Joint Research Center for Advanced Functional Materials  
Zhuhai MUST Science and Technology Research Institute  
Macau University of Science and Technology  
Taipa, Macau 999078, China

Y.-M. Xie  
Jiangsu Key Laboratory of Advanced Negative Carbon Technologies  
Soochow University  
Suzhou, Jiangsu 215123, P. R. China

 The ORCID identification number(s) for the author(s) of this article can be found under <https://doi.org/10.1002/aesr.202300263>.

© 2024 The Authors. Advanced Energy and Sustainability Research published by Wiley-VCH GmbH. This is an open access article under the terms of the Creative Commons Attribution License, which permits use, distribution and reproduction in any medium, provided the original work is properly cited.

DOI: [10.1002/aesr.202300263](https://doi.org/10.1002/aesr.202300263)

perovskite solar cells (OMWPSCs) and all-inorganic wide-bandgap perovskite solar cells (AIWPSCs).<sup>[16,22–24]</sup> Thanks to the intrinsic wide-bandgap and high thermal stability of AIWPSCs, substantial efforts have been dedicated to enhancing the performance of AIWPSCs. As a result, the PCE of AIWPSCs can now surpass that of their OMWPSCs counterparts with the same bandgap.<sup>[25–29]</sup> Despite the significant advancements in AIWPSCs, they still face challenges related to energy loss and phase instability. The low Goldschmidt tolerance factor of all-inorganic perovskites (Figure 1), ranging from 0.815 for  $\text{CsPbBr}_3$  to 0.808 for  $\text{CsPbI}_3$ ,<sup>[14,30–33]</sup> poses a significant obstacle to the development of high-stability AIWPSCs. Especially for  $\text{CsPbI}_3$ , the notably low tolerance factor (0.808) makes it challenging to maintain the black perovskite phase at room temperature.<sup>[34]</sup> Thus, extensive efforts have been directed toward revealing the internal chemical, structural, and electric properties of all-inorganic perovskites.<sup>[35]</sup> In contrast, all-inorganic perovskites also face a challenge related to the high defect density issue caused by complicated crystallization properties, which leads to a further reduced efficiency of AIWPSCs. To address these issues, various strategies have been developed, such as solvent engineering, additive engineering, interface modification, and the exploration of new charge transport materials (CTMs), aiming to enhance the device performance of AIWPSCs by modifying perovskite crystallization properties.<sup>[36]</sup> Although some reviews about all-inorganic PSCs have been reported, these reviews mainly focus on device efficiency. For example, Yuan et al. concluded on various aspects of all-inorganic PSCs, including device efficiency, working principle, structure, characterization methods, preparation process, and simulation software.<sup>[37]</sup> Xiang et al. comprehensively reviewed on the stability of all-inorganic perovskite solar cells,<sup>[38]</sup> and the development of small band gap all-inorganic PSC devices.<sup>[39]</sup> In this review, we comprehensively summarize the development of AIWPSCs, not only encompassing optimization strategies for enhancing device stability and efficiency, but also addressing the challenges aiming to stimulate ideas and inspiration for advancing the field of AIWPSCs.

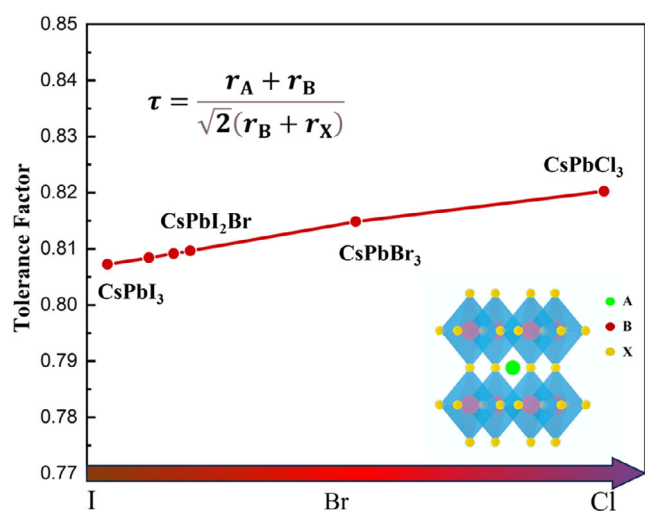


**Figure 1.** Calculated tolerance factors for various halide combinations of commonly employed cesium-based all-inorganic perovskites.

## 1.1. Device Performance Progress

To present a clear view of the recent progress of AIWPSCs, the device characteristics (PCE,  $V_{OC}$ , and  $V_{OC}$  loss) of representative AIWPSCs, reported in recent years, are depicted in Figure 2a–c. It can be seen that all kinds of AIWPSCs have undergone significant advancements in terms of both PCE and  $V_{OC}$ . In line with the perovskite film optical bandgap,  $\text{CsPbI}_3$ -based AIWPSCs have a higher device efficiency than the other AIWPSCs (Figure 2a), which is guaranteed by the broader absorption range of  $\text{CsPbI}_3$  than the other inorganic perovskites. In contrast, the largest bandgap  $\text{CsPbBr}_3$ -based AIWPSCs exhibit the largest  $V_{OC}$  values (Figure 2b). Among the devices,  $\text{CsPbI}_3$ -based AIWPSCs exhibit the most significant increase in PCE, rising from 5.71% in 2017 to 21% in 2022 (Figure 2c),<sup>[40,41]</sup> most notable enhancement in  $V_{OC}$ , increasing from 0.71 V in 2017 to 1.18 V in 2023,<sup>[40,42]</sup> and the most obvious reduction in  $V_{OC}$  loss.

However, apart from the PCE, their high sensitivity to humidity also poses a challenge to the development of high-performance AIWPSCs. Typically, as shown in Figure 3d, all-inorganic perovskites have four types of crystal structures: cubic ( $\alpha$ ), tetragonal ( $\beta$ ), and orthorhombic ( $\gamma$ ) perovskite phases, and non-perovskite phase ( $\delta$ -phase).<sup>[43]</sup> Among them,  $\alpha$ ,  $\beta$ , and  $\gamma$  perovskite phases can convert photons into carriers, whereas the non-perovskite phase (yellow phase) cannot utilize photons and, instead, can induce the collapse of the perovskite phases. Furthermore, the formation of perovskite phases typically requires high annealing temperatures, and maintaining these phases also necessitates elevated temperatures. For example, a high annealing temperature of over 350 °C is required to form the  $\alpha$  phase  $\text{CsPbI}_3$ . As the temperature gradually cools to room temperature, the  $\alpha$  phase undergoes a transformation into the  $\beta$  and  $\gamma$  phases, and may even degrade into the non-perovskite  $\delta$  phase, resulting in seriously deteriorated device performance.<sup>[43]</sup> According to the Goldschmidt tolerance factor ( $\tau$ ) equation

$$\tau = \frac{r_A + r_B}{\sqrt{2}(r_B + r_X)} \quad (1)$$

where  $r_A$ ,  $r_B$ , and  $r_X$  represent the ionic radii for the A, B, and X sites, respectively. The low  $\tau$  value in all-inorganic perovskites, caused by the substitution of organic cations with smaller  $\text{Cs}^+$  ions, is proposed as the primary reason for the phase instability.

Although extensive efforts have been devoted to dealing with this issue, compromised device stability remains a prominent challenge for  $\text{CsPbI}_3$ -based AIWPSCs.<sup>[40–42,44–47]</sup> In contrast, due to the notably high  $\tau$  value (0.815),  $\text{CsPbBr}_3$  exhibits obviously enhanced phase stability, and  $\text{CsPbBr}_3$ -based AIWPSCs have illustrated a lifetime of over 2000 h in ambient air.<sup>[48]</sup> However, the wide bandgap (2.3 eV) of  $\text{CsPbBr}_3$  leads to a limited light-harvesting range (<550 nm) of its based AIWPSCs, which results in confined device efficiency.<sup>[49,50]</sup> Moreover, the fast crystallization process of  $\text{CsPbBr}_3$ , induced by the high affinity of  $\text{Br}^-$  to  $\text{Pb}^{2+}$ , commonly provokes the formation of deep-level defects in the perovskite film, which leads to further deteriorated device performance.<sup>[51–53]</sup> Consequently, bromide ( $\text{Br}^-$ ) and iodide ( $\text{I}^-$ ) mixed all-inorganic perovskites ( $\text{CsPbI}_{x}\text{Br}_{1-x}$ ) are widely adopted owing to their moderate phase stability and relatively wide light-absorption range. Although the crystallization processes of

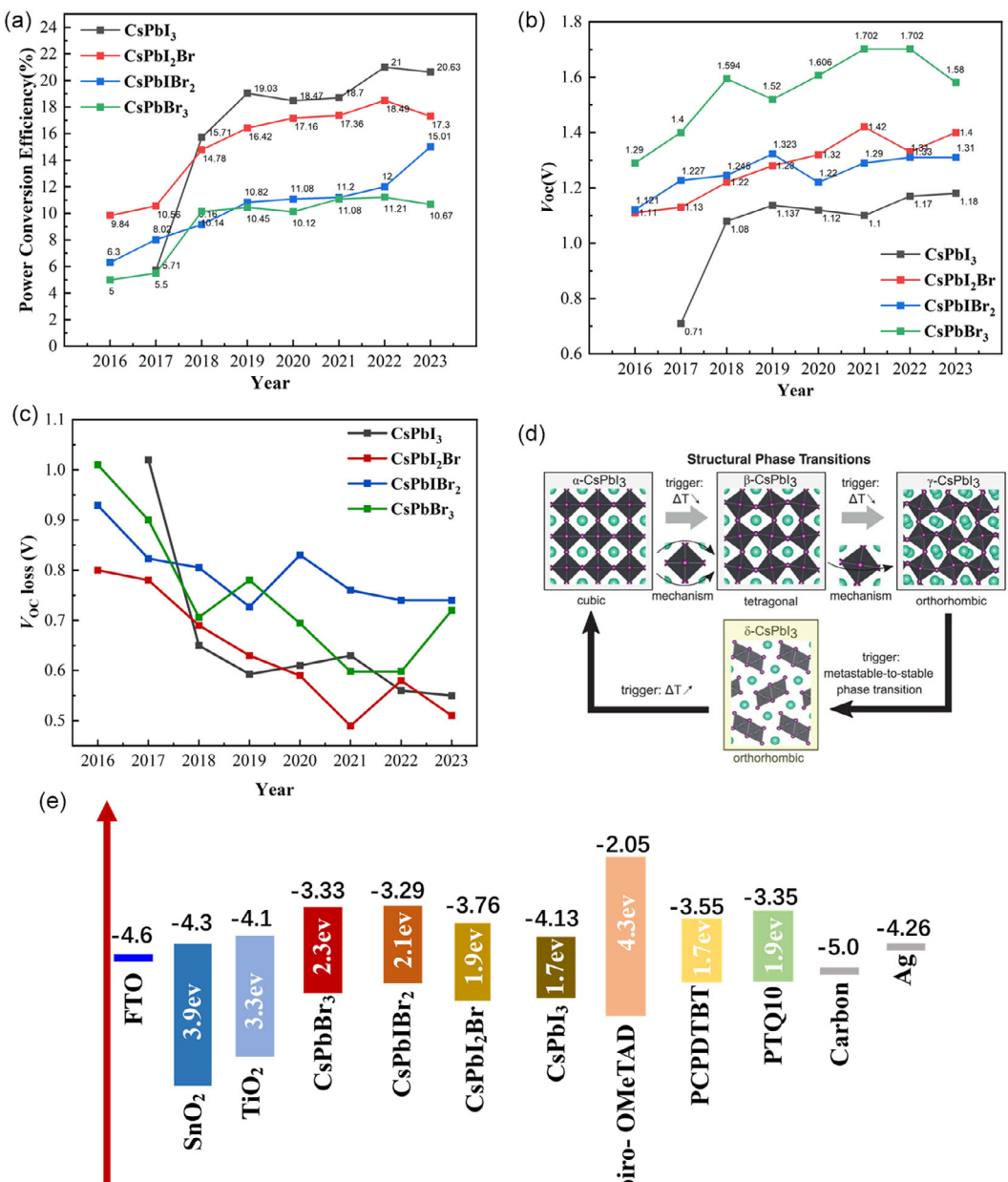


**Figure 2.** a) PCE, b) open-circuit voltage ( $V_{oc}$ ), and c)  $V_{oc}$  loss development of representative AIWPSCs, especially CsPbBr<sub>3</sub>,<sup>[53,102–108]</sup> CsPbI<sub>3</sub>,<sup>[40–42,44–46,109]</sup> CsPbI<sub>2</sub>Br,<sup>[15,110–116]</sup> CsPbIBr<sub>2</sub>,<sup>[117–124]</sup> and CsPbBr<sub>3</sub>. d) Transformation between different crystal phases of CsPbI<sub>3</sub> all-inorganic perovskites. Reprinted with permission.<sup>[43]</sup> Copyright 2019, Science. e) Energy level diagrams of AIWPSCs with different perovskite components.

CsPbI<sub>x</sub>Br<sub>1-x</sub> can be modulated by adjusting the halide composition, it is important to note that a high thermal annealing temperature exceeding 200 °C is still required.<sup>[47,54–56]</sup> Therefore, high thermal durability CTMs are chosen as the charge transport layers (CTLs) for the perovskite film underlayer. However, there are rarely reported organic hole transport materials (HTMs) and electron transport materials (ETMs) that can undergo a high annealing temperature of over 200 °C. As a result, almost all the all-inorganic perovskite films are deposited onto metal oxide CTLs (such as ZnO, SnO<sub>2</sub>, and TiO<sub>2</sub>), and most

AIWPSCs are SnO<sub>2</sub> based n-i-p structured devices.<sup>[22,23,57,58]</sup> However, the relatively deeper conduction band (CB) of SnO<sub>2</sub> than the lowest unoccupied molecular orbital (LUMO) level of inorganic perovskite films (ranging from -4.13 eV for CsPbI<sub>3</sub> to -3.33 eV for CsPbBr<sub>3</sub>, Figure 2e) poses an obstacle for electron transport,<sup>[22,23]</sup> which hinders the development of high-efficiency AIWPSCs. Therefore, effective perovskite crystallization modulating strategies and high-performance CTLs with suitable energy levels and excellent thermal stability are also highly desired.

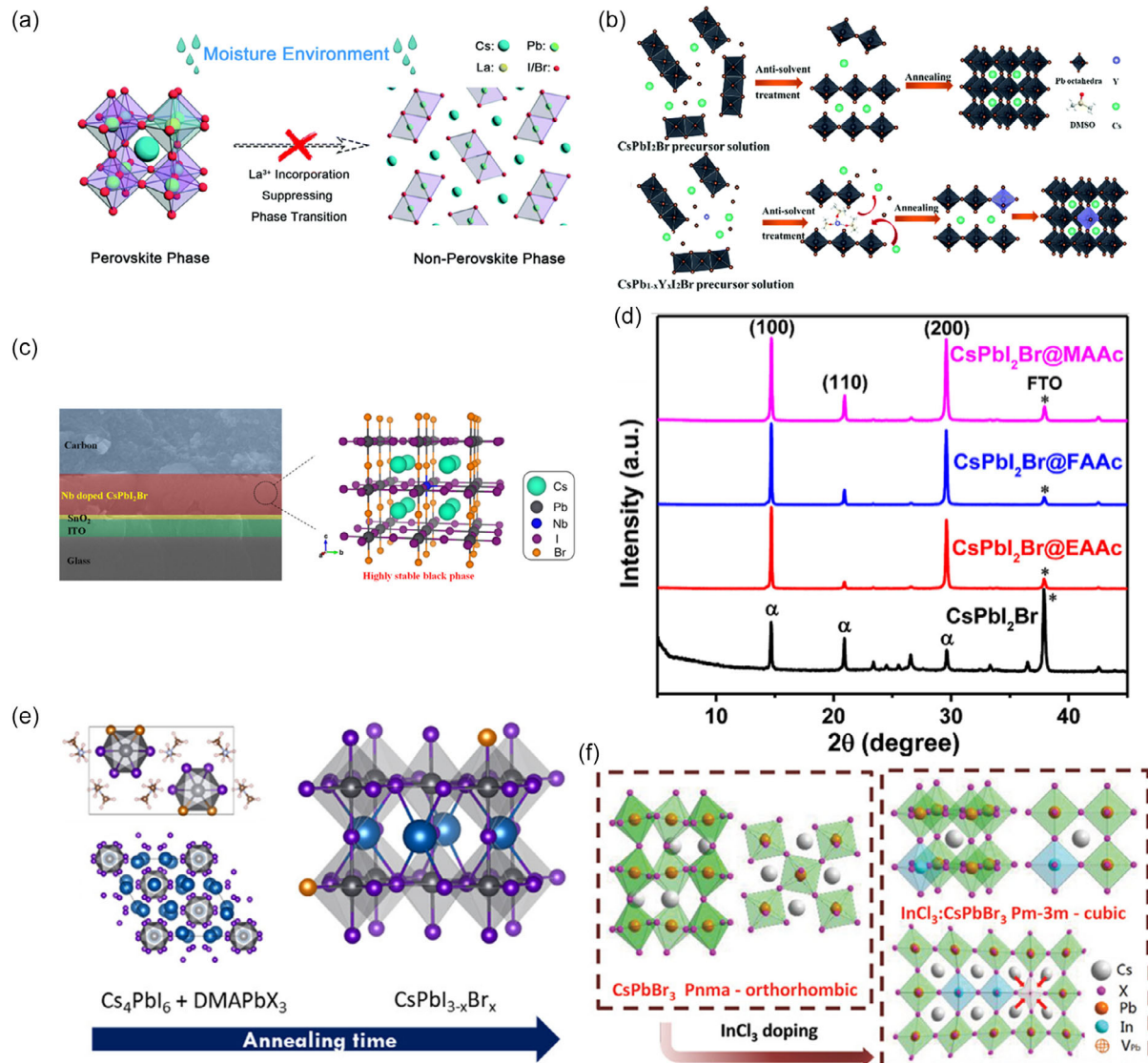


**Figure 3.** a) Schematic diagram of the pristine  $\text{CsPbI}_2\text{Br}$  and  $\text{La}^{3+}$ -doped  $\text{CsPb}_{1-x}\text{La}_x\text{I}_2\text{Br}$  perovskite phase stability in a moist environment.<sup>[62]</sup> Copyright 2020, The Royal Society of Chemistry. b)  $\text{CsPbI}_2\text{Br}$  perovskite crystallization and yttrium-induced crystallization engineering involving yttrium-DMSO intercalated between  $[\text{PbI}_6]$  octahedral layers. Reprinted with permission.<sup>[63]</sup> Copyright 2019, The Royal Society of Chemistry. c)  $\text{CsPb}_{1-x}\text{Y}_x\text{I}_2\text{Br}$ -based AIWPSCs. Reprinted with permission.<sup>[64]</sup> Copyright 2019, American Chemical Society. d) XRD patterns of  $\text{CsPbI}_2\text{Br}$  thin films prepared from different precursors. Reprinted with permission.<sup>[57]</sup> Copyright 2022, Elsevier. e) Representation of the intermediate phases and their evolution during annealing to form  $\text{CsPbI}_{3-x}\text{Br}_x$ . Dark gray, purple, orange, blue, light gray, and light brown balls represent lead, iodine, bromine, cesium, nitrogen, and carbon, respectively. Reprinted with permission.<sup>[68]</sup> Copyright 2023, Wiley-VCH GmbH. f) Evolution of the crystal structure and space group of  $\text{CsPbBr}_3$  single crystal with the  $\text{InCl}_3$  dopant. Reprinted with permission.<sup>[69]</sup> Copyright 2018, Wiley-VCH GmbH.

## 2. Additive Engineering

As mentioned above, although all-inorganic perovskites ( $\text{CsPbX}_3$ ) have been demonstrated with superb thermal stability, their high sensitivity to humidity poses a challenge to the development of high-performance AIWPSCs. Among the employed methods, additive engineering is a widely adopted strategy owing to the interaction between the specific functional groups of the additives to passivate perovskite defects as well as the effect on enhancing perovskite crystallinities.

As depicted in Figure 1, with the increasing of small size ion  $\text{Br}^-$  (1.96 Å) ratio, the  $\tau$  value also gradually increases, which can contribute to the enhanced phase stability of all-inorganic perovskites.<sup>[59]</sup> McGehee et al. reported that to attain a stable perovskite phase at room temperature, it is necessary to substitute a minimum of 30% of the larger  $\text{I}^-$  ions (2.2 Å) in  $\text{CsPbI}_3$  with  $\text{Br}^-$  to achieve good perovskite phase stability at room temperature.<sup>[60]</sup> However, the introduction of  $\text{Br}^-$  will lead to an increased bandgap of the perovskite film, thereby sacrificing the absorption of the longer wavelength part of sunlight.<sup>[61]</sup>

ultimately compromising the device efficiency. Therefore, strategies for maintaining all-inorganic perovskite phase stability, especially the phase stability of  $\text{CsPbI}_3$ , are highly desired. Aside from the replacement of  $\text{I}^-$  with  $\text{Br}^-$ , the tolerance factor can be enhanced by changing the ionic radius of the A-site or the B-site. For example, the introduction of lanthanum ions ( $\text{La}^{3+}$ ) can effectively enhance the moisture stability of  $\text{CsPbI}_2\text{Br}$  perovskite devices by inducing shrinkage of the perovskite lattice (Figure 3a).<sup>[62]</sup> It has been found that partial substitution of  $\text{Pb}^{2+}$  with yttrium ions ( $\text{Y}^{3+}$ ) can lead to the host lattice rearrangement of perovskites, which can enable a more favorable  $\tau$  value for maintaining the perovskite phase than the control film (Figure 3b).<sup>[63]</sup> The prepared  $\text{CsPb}_{1-x}\text{Y}_x\text{I}_2\text{Br}$ -based AIWPSCs exhibit no PCE decrease in humid air with 65% RH. Furthermore, by substituting a fraction of the divalent lead ions with  $\text{Nb}^{3+}$  ions, the all-inorganic PSC, utilizing a carbon electrode, achieves remarkable moisture stabilization capabilities when subjected to 0.5%  $\text{Nb}^{3+}$  doping (Figure 3c).<sup>[64]</sup> It should be noted that the doping concentration of B-site elements is usually maintained at less than 1% to ensure that the original perovskite lattice structure is not destroyed.

Different from B-site doping, organic materials can also be adopted in A-site doping for the fabrication of high-quality all-inorganic perovskites by facilitating the formation of an intermediate perovskite phase. Ho-Baillie et al. reported a simple cation-exchange-growth (CEG) method for achieving high-quality  $\text{CsPbI}_3$  films by introducing the additional organic cation methylammonium ( $\text{MA}^+$ ) in the all-inorganic precursor solution.<sup>[65]</sup> It has been observed that  $\alpha\text{-MAPbI}_3$  is previously formed at the beginning of the crystallization process, then,  $\text{Cs}^+$  will be inserted into the perovskite crystal by substituting  $\text{MA}^+$  without changing the crystal phase. As a result, a pure  $\alpha\text{-CsPbI}_3$  perovskite film is achieved, based on which a high PCE of 14.4% is achieved. Luo et al. reported a method involving formamidine acetate (FAAc) organic dopant in the preparation of high-quality  $\gamma\text{-CsPbI}_3$  perovskite films.<sup>[66]</sup> It has been revealed that the incorporation of FAAC into perovskite precursor solution can alter the phase transition process with an additional intermediate phase, and the replacement of  $\text{FA}^+$  with  $\text{Cs}^+$  leads to an optimized crystallinity of the  $\gamma\text{-CsPbI}_3$  film, which promotes a PCE over 18% for AIWPSCs. Another crucial point to improve the quality of all-inorganic perovskite films is crystallization process regulation. During the formation of the yellow phase and the process of rapid crystallization, additives can play a very effective role in regulating perovskite crystallization properties. A study by Yu et al. showed that the introduction of FAAC in  $\text{CsPbI}_2\text{Br}$  could derive a phase-pure  $\text{CsFA}_{0.5}\text{PbI}_2\text{BrAc}_{0.5}$  intermediate phase. Based on this strategy, unfavorable phase transitions during the crystallization of  $\text{CsPbI}_2\text{Br}$  were prevented, and high-quality perovskite films were achieved with a high PCE of 16.36% (Figure 3d).<sup>[57]</sup> Che et al. found that both the reduction of defect density and the stabilization of the perovskite phase of  $\text{CsPbI}_3$  can be obtained through the introduction of hydrazide derivatives benzoyl hydrazine (BH), formohydrazide (FH), and benzamide (BA).<sup>[67]</sup> Zhao and his colleagues made a noteworthy discovery by introducing an efficient volatile additive, dimethylammonium iodide (DMAI), into the  $\text{CsPbI}_3$  precursor solution to modulate the crystallization process.<sup>[45]</sup> The optimal film guarantees a record device efficiency of 19.03% with high stability.

Moreover, Montecucco and his team identified that DMAX (dimethylammonium xanthate) can also be employed to fine-tune the crystallization process of all-inorganic perovskite by lowering the annealing temperature, showcasing the versatility and effectiveness of this approach in diverse contexts (Figure 3e).<sup>[68]</sup> Mai et al. showed that the introduction of the inorganic indium chloride ion ( $\text{InCl}_3$ ) dopant into the lattice structure of inorganic  $\text{CsPbI}_2\text{Br}$  can also help to inhibit the formation of the yellow phase (Figure 3f).<sup>[69]</sup> This modification enables AIWPSCs to maintain their efficiency for up to 80 h in ambient air without any degradation. Jong et al. reported  $\text{Cs}^+$  and rubidium ( $\text{Rb}^+$ ) mixed all-inorganic perovskites  $\text{Cs}_{1-x}\text{Rb}_x\text{PbI}_3$  with modified phase stability.<sup>[70]</sup> Their research revealed that compared with the two end pure compounds  $\text{CsPbI}_3$  and  $\text{RbPbI}_3$ ,  $\text{Cs}_{1-x}\text{Rb}_x\text{PbI}_3$  was more stable at room temperature due to the increase in configurational entropy. Kim et al. found that partial substitution of  $\text{Cs}^+$  with potassium ( $\text{K}^+$ ) can effectively enhance the inorganic perovskite phase stability and crystallinity without changing the crystal structure.<sup>[71]</sup> Tian et al. found that perovskite can be passivated by introducing excess lead iodide ( $\text{PbI}_2$ ), which can reduce the charge recombination among the perovskite grains through the charge-blocking effect.<sup>[58]</sup> Moreover,  $\text{CsPbI}_2\text{Br}$  film with modified optoelectronic performance can also be obtained by adding  $\text{FeCl}_2$  into the composition to modulate the tolerance factor of perovskites.<sup>[72]</sup>

Additionally, it has been discovered that the inclusion of self-assembled molecule (SAM) additives can also promote the formation of high-quality all-inorganic perovskite films. Ma et al. reported the effect of SAM cation guanidinium (GA) on passivating all-inorganic perovskites.<sup>[73]</sup> It has been revealed that the three symmetric amino groups of the cation can interact with the uncoordinated Pb defects, resulting in the fabrication of high-quality all-inorganic perovskite films with inhibited defect states (Figure 4a). Furthermore, Song et al. found that the addition of thiethylmethylamine acetate (ThMAAc) can facilitate the formation of the  $\alpha$  phase while impeding the formation of the yellow phase in  $\text{CsPbI}_2\text{Br}$  (Figure 4b).<sup>[74]</sup> By adding ThMAAc into perovskite precursor solutions, high-quality all-inorganic perovskite films with reduced defect states and modified surface morphologies are obtained, which leads to modified perovskite/HTL interface properties. Ultimately, resulting in an increased device efficiency from 13.2% for the control device to 14.8%.

In addition to SAM additives, 2D materials have also been found to be favorable additives for passivating all-inorganic perovskites. By introducing phenylethylammonium bromide (PEABr) and  $\text{CsBr}$  into  $\text{CsPbI}_2\text{Br}$ , He. et al. fabricated high-quality  $\text{CsPbI}_2\text{Br}$  film with passivated defects, which promoted a high PCE of 16.7% (Figure 4c).<sup>[75]</sup> Additionally, the introduction of 2D organic cations can also lead to adjustments in the perovskite film morphology, thereby further improving the performance of AIWPSCs. Bahadur et al. found that the incorporation of the 2D material phenethylammonium iodide (PEAI) can also lead to modified uniformity and crystallinity of all-inorganic perovskite films via the formation of the intermediate phase of  $\text{PbX}_2\text{-DMSO}$ : DMF- $\text{CsI}$ -PEAI (Figure 4d).<sup>[76]</sup> Based on the optimized film, a high efficiency of 17.4% was obtained. By adding  $\text{Pb}(\text{Ac})_2$  coordinated with DMSO and  $\text{PbI}_2$ , the formation of the complex  $\text{PA}(\text{Ac})_2\text{-DMSO-PbI}_2$  in the precursor can

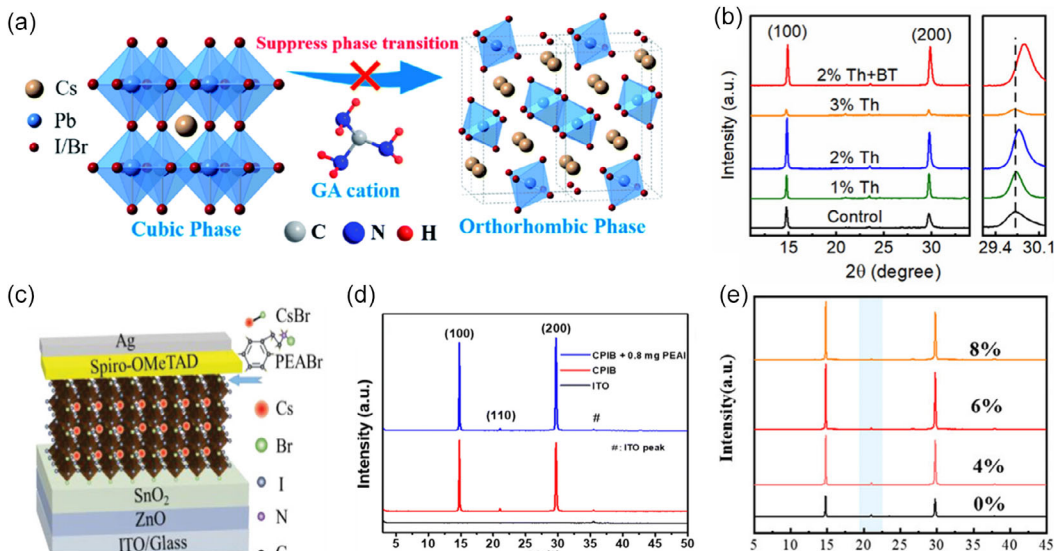


**Figure 4.** a) Schematic illustration of suppressing the phase transition by introducing GA cations. Reprinted with permission.<sup>[73]</sup> Copyright 2019, The Royal Society of Chemistry. b) XRD patterns of thienylmethylamine acetate (ThMAAc) modified all-inorganic perovskite films (from 0% to 3%). Reprinted with permission.<sup>[74]</sup> Copyright 2022, Wiley-VCH GmbH. c) Structure of the CsPbI<sub>2</sub>Br device passivated by PEABr and CsBr. Reprinted with permission.<sup>[75]</sup> Copyright 2021, Wiley-VCH GmbH. d) XRD patterns of CPIB (CsPbI<sub>2</sub>Br) and CPIB + 0.8 mg PEAI perovskite films. Reprinted with permission.<sup>[76]</sup> Copyright 2023, The Royal Society of Chemistry. e) XRD patterns of the film with different contents of Pb(Ac)<sub>2</sub>. Reprinted with permission.<sup>[77]</sup> Copyright 2022, Wiley-VCH GmbH.

provide an intermediate phase for nucleation and crystallization of the perovskite film due to its passivation ability to the defects of iodine and grain boundaries. As a result, the performance of CsPbI<sub>2</sub>Br devices can be effectively improved (Figure 4e).<sup>[77]</sup>

Despite the development of various additives for passivating all-inorganic perovskites, it is important to note that these materials still face challenges related to compromised crystallinity and poor phase stability. Additive engineering is the most widely adopted strategy for modifying perovskite crystallization properties. It is believed that the development of additives such as SAMs and two-dimensional perovskite materials, high-quality all-inorganic perovskite films with enhanced phase stability and PCE can be achieved. Hence, there is a significant demand for additives with exceptional perovskite passivation capabilities to address these challenges and improve the performance of all-inorganic perovskites.

## 2.1. Solvent Engineering

Solvent engineering is recognized as one of the most fundamental methods to fabricate high-quality perovskite films and has been extensively studied for optimizing all-inorganic perovskite properties. The solubility of Br<sup>-</sup> in the most commonly used solvent, N, N-dimethylformamide (DMF), is limited to 0.43 M,<sup>[78]</sup> resulting in a confined precursor concentration, which, in turn, restricts the achieved film thickness of the deposited all-inorganic perovskite film and consequently constrains the light absorption of AIWPSCs. To address this issue, Chen et al. intentionally introduced dimethyl sulfoxide (DMSO) into the precursor solution aiming at increasing the solubility of Br<sup>-</sup> and precursor

concentration.<sup>[78]</sup> The increased precursor concentration (1.15 M) promotes a substantial improvement in the thickness of perovskite films, which allows it to reach 410 nm, while also noticeably enhancing the light absorption intensity. You et al. found that the high boiling point (189 °C) of DMSO can slow the solvent evaporation rate, which can promote ion transmission and diffusion during the annealing process, which can enhance the chemical composition homogeneity of the CsPbI<sub>3</sub> crystals and therefore enhance the phase stability of perovskites.<sup>[44]</sup> As a result, based on the obtained high-quality CsPbI<sub>3</sub> perovskite film, for the first time, a PCE exceeding 15% is achieved for AIWPSCs. Moreover, Zai et al. found that the DMF/DMSO mixed ratio has a profound influence on the crystallization properties of all-inorganic perovskite films, especially the film morphology (Figure 5a).<sup>[79]</sup> It has been found that a high DMF content will cause fast solvent volatilization and lead to a small perovskite grain size and high density. Conversely, high DMSO content will induce the formation of a large number of pinholes due to the larger surface tension, and the perovskite film has optimized crystallization properties when the DMF:DMSO ratio is 2:1. However, it is worth noting that traditional solvents such as DMSO and DMF are known to be toxic and often demand stringent conditions for film formation. Hence, there is a growing need for the development of environmentally friendly solvents for perovskite film fabrication. Wang et al. demonstrated that methylammonium acetate (MAAc) can serve as an excellent environmentally friendly solvent for CsPbI<sub>3-x</sub>Br<sub>x</sub>.<sup>[80]</sup> The strong coordination of the MA<sup>+</sup> and Ac<sup>-</sup> groups to the precursor materials enables the formation of stabilized β-CsPbI<sub>3</sub> films (Figure 5b). By adopting MAAC as the solvent, Lv et al. achieved a high PCE of 18.90% for CsPbI<sub>3</sub>-based AIWPSCs (Figure 5c).<sup>[81]</sup> In addition to ionic liquids, water can also serve as a solvent for

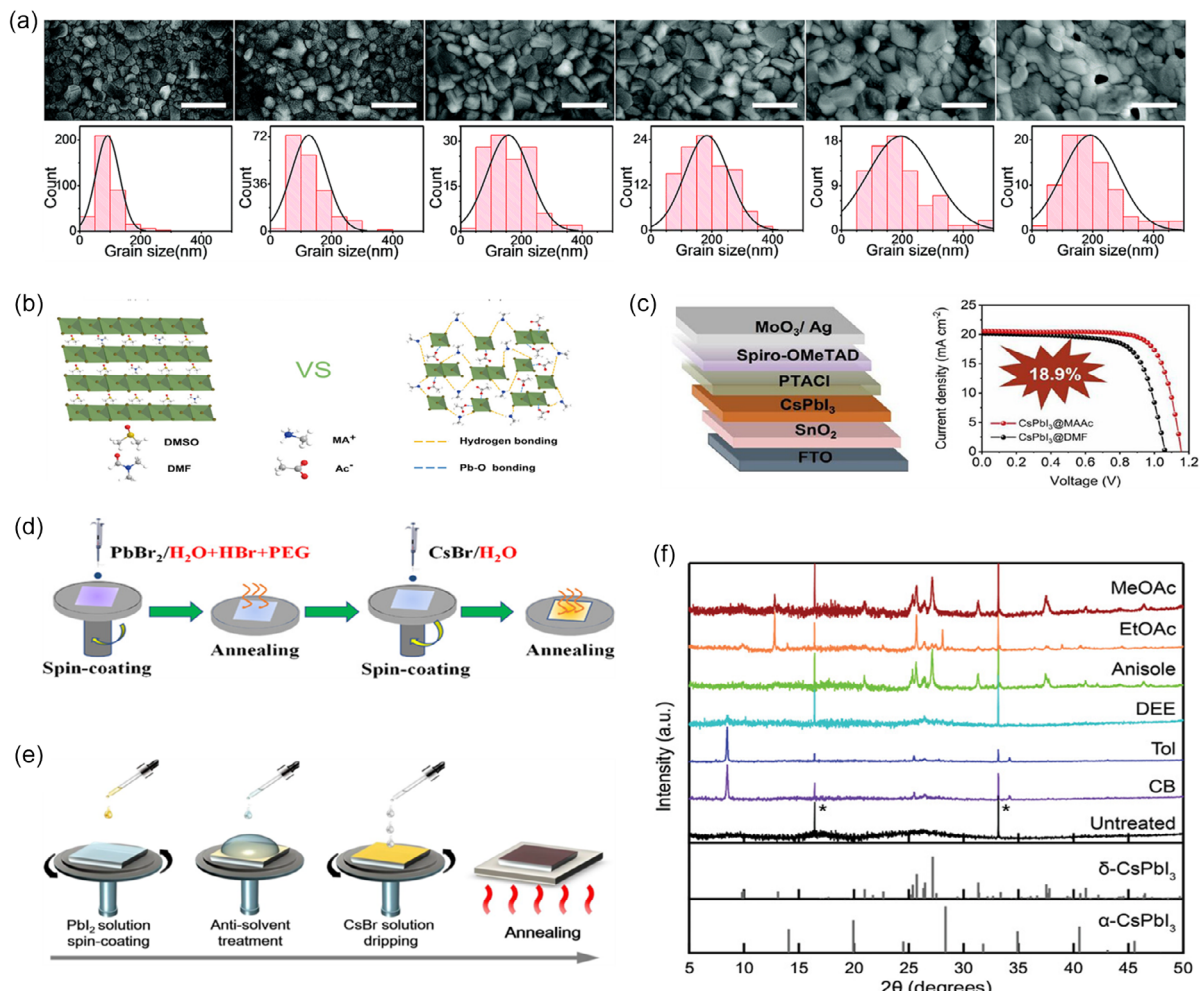


**Figure 5.** a) Top-view SEM images and grain size distribution histograms of the DMF: DMSO = 4:1, 3:1, 2:1, 1:1, 1:2, and 0:1 samples. The scale bar is 500 nm. Reprinted with permission.<sup>[79]</sup> Copyright 2018, The Royal Society of Chemistry. b) Interactions of all-inorganic precursors with DMF:DMSO and methylammonium acetate (MAAc) solvents. Reprinted with permission.<sup>[80]</sup> Copyright 2020, Wiley-VCH GmbH. c) Schematic diagram of the device structure and J-V curves of CsPbI<sub>3</sub>-based AIWPSCs. Reprinted with permission.<sup>[81]</sup> Copyright 2023, American Chemical Society. d) Schematic diagram of the fabrication process of high-quality CsPbBr<sub>3</sub> films from aqueous solutions. Reprinted with permission.<sup>[82]</sup> Copyright 2021, American Chemical Society. e) XRD patterns of unannealed films without antisolvent and with various antisolvent treatments, where \* denotes the quartz substrate peak and the background amorphous peak from the air-free holder was subtracted out with the ICSD XRD pattern for δ-CsPbI<sub>3</sub>, and α-CsPbI<sub>3</sub> (gray). Reprinted with permission.<sup>[18]</sup> Copyright 2020, Wiley-VCH GmbH. f) Schematic illustration of antisolvent-assisted multistep deposition method for fabricating CsPbI<sub>2</sub>Br inorganic perovskite films. Reprinted with permission.<sup>[84]</sup> Copyright 2019, Elsevier.

perovskite fabrication. Ding et al. employed a two-step method, where they first formed a PbBr<sub>2</sub> precursor film using an HBr/H<sub>2</sub>O solution with the addition of ethylene glycol. Following spin-coating of a high-concentration CsBr/H<sub>2</sub>O solution (Figure 5d), high-quality CsPbBr<sub>3</sub> perovskite films were obtained, which delivered a PCE of 7.19%.<sup>[82]</sup> Furthermore, Pang et al. found that by adopting isopropanol (IPA) as the solvent, the reaction temperature between DMAPI<sub>3</sub> and Cs<sub>4</sub>PbI<sub>6</sub> toward CsPbI<sub>3</sub> can be reduced to 100 °C.<sup>[83]</sup> The prepared perovskite films facilitated the fabrication of AIWPSCs with a PCE value of over 16%, which can retain over 93% of the initial value after 30 d of exposure to ambient air.

In addition to the solvent modulation method, the selection of the antisolvent can also improve the morphology and conditions of film crystallization, thereby enhancing the quality of

perovskite crystal films. Wang et al. presented a multistep deposition strategy assisted by an antisolvent for the fabrication of high-quality CsPbI<sub>2</sub>Br films (Figure 5e).<sup>[84]</sup> It has been well-established that antisolvents can aid in the creation of porous PbI<sub>2</sub> (DMSO) films. Subsequently, through the interaction between the CsBr solution and the porous film, along with further control over the target components and film morphology, researchers were able to achieve a device with an efficiency of 10.21% based on the CsPbI<sub>2</sub>Br film. Moreover, for the first time, Luther et al. comprehensively compared various antisolvents (CB, toluene, MeOAc, DEE, anisole, EtOAc) in inorganic perovskite compositions.<sup>[18]</sup> They proposed that A-site plays a critical role in interacting with antisolvents during the crystallization process. By carefully characterizing the crystallization properties of al-inorganic perovskite films, MeOAc was chosen for assisting

crystallization owing to its capability to form the CsI-MeOAc intermediate phase (Figure 5f) during the crystallization process, which is favorable for achieving high-quality  $\text{CsPbI}_3$  films with enhanced crystallinity. Recently, Yang et al. proposed that a mixed antisolvent of CB and IPA can realize low-temperature fabrication of  $\text{CsPbIBr}_2$  ( $150^\circ\text{C}$ ), and the PCE can achieve 8.48% by using the device structure of FTO/TiO<sub>2</sub>/CsPbIBr<sub>2</sub>/ZnPc/carbon.<sup>[85]</sup>

As mentioned above, the choice of solvent for the perovskite precursor solution significantly impacts the crystallization properties of all-inorganic perovskite films. Studies have revealed that the mixing ratio between two mostly adopted solvents, DMF and DMSO, has a profound impact on the solvent volatilization rate of the spin-coated film. Furthermore, by carefully selecting the anti-solvent, the crystallization process of all-inorganic perovskites can be effectively modulated. Nevertheless, the toxicity of these solvents leads to an adverse effect on the environment, which provokes the exploration of green solvents for perovskites. However, up to now, the green solvents-based AIWPSCs have compromised performance than that fabricated with DMF and DMSO mixed solvents, and investigations on prominent green solvents for AIWPSCs remain needed.

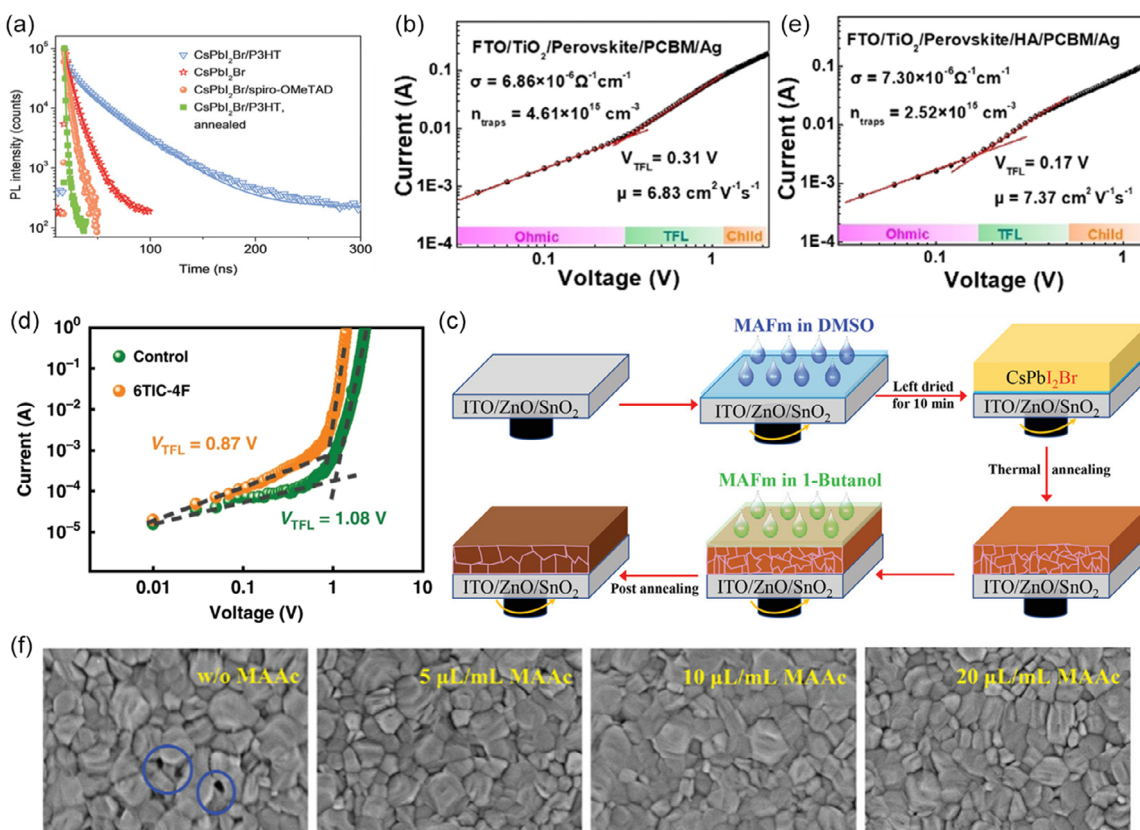


**Figure 6.** a) Photoluminescence (PL) decay curves for  $\text{CsPbI}_2\text{Br}$ ,  $\text{CsPbI}_2\text{Br}/\text{spiro-OMeTAD}$ ,  $\text{CsPbI}_2\text{Br}/\text{P}3\text{HT}$ , and annealed  $\text{CsPbI}_2\text{Br}/\text{P}3\text{HT}$  samples.<sup>[89]</sup> Copyright 2018, Wiley-VCH GmbH. Trap density within the all-inorganic perovskite films b) without and c) with HA passivation. Reprinted with permission.<sup>[90]</sup> Copyright 2021, Wiley-VCH GmbH. d) J-V characteristics of AIWPSCs with the configuration of ITO/SnO<sub>2</sub>/ $\text{CsPbI}_{3-x}\text{Br}_x$ /ZnO/Ag for estimating the defect density in the perovskite films. Reprinted with permission.<sup>[91]</sup> Copyright 2020, Nature. e) XRD patterns of the target perovskite film with different annealing times and schematic diagram of the formation process of the target BHJ film. Reprinted with permission.<sup>[92]</sup> Copyright 2023, American Chemical Society. f) Schematic diagrams of the preparation and postprocessing process of the modified  $\text{CsPbI}_2\text{Br}$  films with MAFm. Reprinted with permission.<sup>[23]</sup> Copyright 2023, Wiley-VCH GmbH. g) Scanning electron microscopy (SEM) images of  $\text{CsPbI}_{2.2}\text{Br}_{0.8}$  films without MAAC and with 5, 10, and 20  $\mu\text{L mL}^{-1}$  MAAC. Reprinted with permission.<sup>[22]</sup> Copyright 2023, Wiley-VCH GmbH.

exhibits a high open-circuit voltage ( $V_{OC}$ ) of 1.32 V and a high PCE of 12.1%. Tan et al. reported a straightforward method for fabricating high-quality  $\text{CsPbI}_3$  films. They introduced an inorganic additive, ammonium halide (HA), into the precursor solution.<sup>[47]</sup> Gu et al. discovered that HA can heal iodine vacancies (V1) on the interface of the perovskite film through a Lewis base–acid interaction, which contributes to an effectively reduced interface trap density (Figure 6b,c).<sup>[90]</sup> Huo et al. employed propylamine hydrobromide (PABr) and its derivative 3-bromopropylamine hydrobromide (3Br-PABr) to passivate the interface defects of carbon-based  $\text{CsPbI}_2\text{Br}$  perovskite films, and finally, a PCE of 14.04% was achieved.<sup>[86]</sup> Yip and his coworkers found that the nitrile (C-N) group in the Lewis base small molecule (6TIC-4F) can passivate the Pb-exposed interface to reduce the trap density of the  $\text{CsPbI}_x\text{Br}_{3-x}$  film, leading to a reduction in trap density within the perovskite film (Figure 6d).<sup>[91]</sup> As a result, the charge extrication efficiency at the perovskite/CTL interface is significantly enhanced, which leads to a champion PCE of 16.1%. Furthermore, Kang et al. reported a strategy for synthesizing 2D/3D  $\text{CsPbI}_4\text{Br}/\text{CsPbI}_2\text{Br}$  bulk heterojunction (BHJ) all-inorganic perovskites by adding excessive lead iodide to the precursor solution. In this approach, the 2D layer can effectively passivate the surface defects distributed at the surface of the 3D  $\text{CsPbI}_2\text{Br}$  film (Figure 6e).<sup>[92]</sup> Moreover, Fu and coworkers proposed that the treatment of all-inorganic perovskite interfaces with 4,4'-dimethoxytriphenylmethyl chloride (DMT-Cl) is not only beneficial for inhibiting the interface defects of perovskites, but also favorable for enhancing the stability of all-inorganic perovskites in wet environments.<sup>[93]</sup> In contrast, the treatment of the all-inorganic perovskite film surface with  $\text{CH}_3\text{NH}_3\text{Nr}$  (MABr) can induce a recrystallization process with the perovskite film, contributing to the formation of large grain size perovskite films with full coverage.<sup>[94]</sup> Previously, we found that the introduction of MAAc at the perovskite bottom layer can facilitate the fabrication of high-quality uniform all-inorganic perovskites with enhanced crystallinity, which promotes a high PCE of 17.16% and an open circuit voltage ( $V_{OC}$ ) of 1.31 V (Figure 6f).<sup>[22]</sup> After that, methylammonium formate (MAFm) is further adopted as a dual-interface modulator to passivate both of the top and bottom interfaces of all-inorganic perovskite films (Figure 6g).<sup>[23]</sup> We found that dual-interface modification can not only optimize the film morphology but also enlarge the perovskite grain size, which is beneficial for mitigating the perovskite grain boundary defects and accelerating charge extraction. As a result, high-efficiency AIWPSCs with a PCE of 17% and a high opening voltage of 1.347 V were obtained.

As discussed above, the properties of the perovskite/CTL interface have a significant impact on the performance of AIWPSCs. Interface treatment is crucial for regulating the charge extraction and transport processes in AIWPSCs. Despite various methods proposed to passivate perovskite surface defects and optimize interface properties, energy loss still occurs at the perovskite/CTL interfaces. Therefore, there is a strong need for efficient strategies to mitigate this interface energy loss. It is proposed that, with the development of CTls, particularly CTls with strong perovskite passivation effect and suitable energy level alignment with the perovskite film, the energy loss at the perovskite/CTL interface can be effectively minimized.

#### 4. New Charge Transport Layer

As sandwich-structured, multilayered devices, the charge transport properties from CTls to their connected electrodes also play a pivotal role in influencing the performance of AIWPSCs. According to the material function, CTMs can be categorized into two groups: ETMs and HTMs. The key function of CTls is to create selective contacts. Specifically, the ETL primarily focuses on extracting electrons from perovskite films, transporting them to the cathode, and hindering hole transport, while the HTL serves the opposite purpose. However, due to the broad bandgap (>1.7 eV) of all-inorganic perovskite films, it is challenging to find CTls (HTL and ETL) with compatible energy levels (HOMO and LUMO). Consequently, high energy loss ( $E_{loss} = E_g - eV_{OC}$ ) happens in AIWPSCs, thus compromising device efficiency.<sup>[95]</sup> Therefore, to more precisely control the charge dynamics in AIWPSCs and further improve device efficiency, it is of utmost importance to explore suitable CTMs for AIWPSCs.

Due to its high thermal stability, high electron mobility, and good antireflection,  $\text{SnO}_2$  has become one of the most popular ETMs for AIWPSCs. In contrast, Chang et al. discovered that  $\text{ZnO}$  is a superior ETL material for all-inorganic perovskite. They achieved an outstanding PCE of 14.78% with a high  $V_{OC}$  of 1.21 V.<sup>[96]</sup> Moreover, Yip et al. found that the insertion of the higher-lying conduction band minimum (CBM) ETL  $\text{ZnO}$  (-4.21 eV) at the  $\text{SnO}_2/\text{perovskite}$  interface can facilitate the establishment of a desirable cascade energy level alignment between the  $\text{CsPbI}_2\text{Br}$  film and  $\text{SnO}_2/\text{ZnO}$  bilayered ETL (Figure 7a), which contributes to suppressed perovskite/ETL interfacial trap-assisted recombination with lower charge recombination rate and higher charge extraction efficiency.<sup>[97]</sup> Moreover, this bilayered ETL possesses a stronger electron extraction capability than the single-layer metal oxide ETL ( $\text{SnO}_2$  and  $\text{ZnO}$ ), which improves the  $V_{OC}$  from 1.06 V for the control device to 1.23 V.

Although the existing ETMs have compromised optoelectronic properties, the confined choices of the materials for synthesizing metal oxide ETMs narrow their compositions. To date,  $\text{ZnO}$ ,  $\text{SnO}_2$ , and  $\text{NiO}_x$  remain the primary metal oxide ETMs for AIWPSCs. Therefore, more efforts are directed at discovering high-performance HTMs for AIWPSCs. Among the HTMs, 2,2',7,7'-tetrakis(*N,N*-di-*p*-methoxyphenylamine)-9,9'-spirobifluorene (spiro-OMeTAD) is one of the most widely adopted materials for AIWPSCs. Nevertheless, the high production cost and limited stability of spiro-OMeTAD have impeded the development of high-performance AIWPSCs. Consequently, considerable efforts have been dedicated to identifying high-quality HTM candidates to replace spiro-OMeTAD.<sup>[95,97–100]</sup> Li et al. found that poly[2,6-(4,4-bis(2-ethylhexyl)-4 H-cyclopenta[2,1-b;3,4-b]dithiophene)-alt-4,7-(2,1,3-benzothiadiazole)] (PCPDFTBT) can replace spiro-OMeTAD to serve as the HTL for  $\text{CsPbI}_2\text{Br}$  (Figure 7b).<sup>[98]</sup> It has been observed that PCPDFTBT can not only enhance hole extraction and transportation efficiency but also, due to its hydrophobic properties, contribute to the improved humidity durability of all-inorganic perovskites. Zhou et al. reported that the low-cost polymer poly[(thiophene)-alt-(6,7-difluoro-2-(2-hexyldecoxy)quinoxaline)] (PTQ10) can also serve as a suitable HTM for AIWPSCs owing to its better energy level matching between

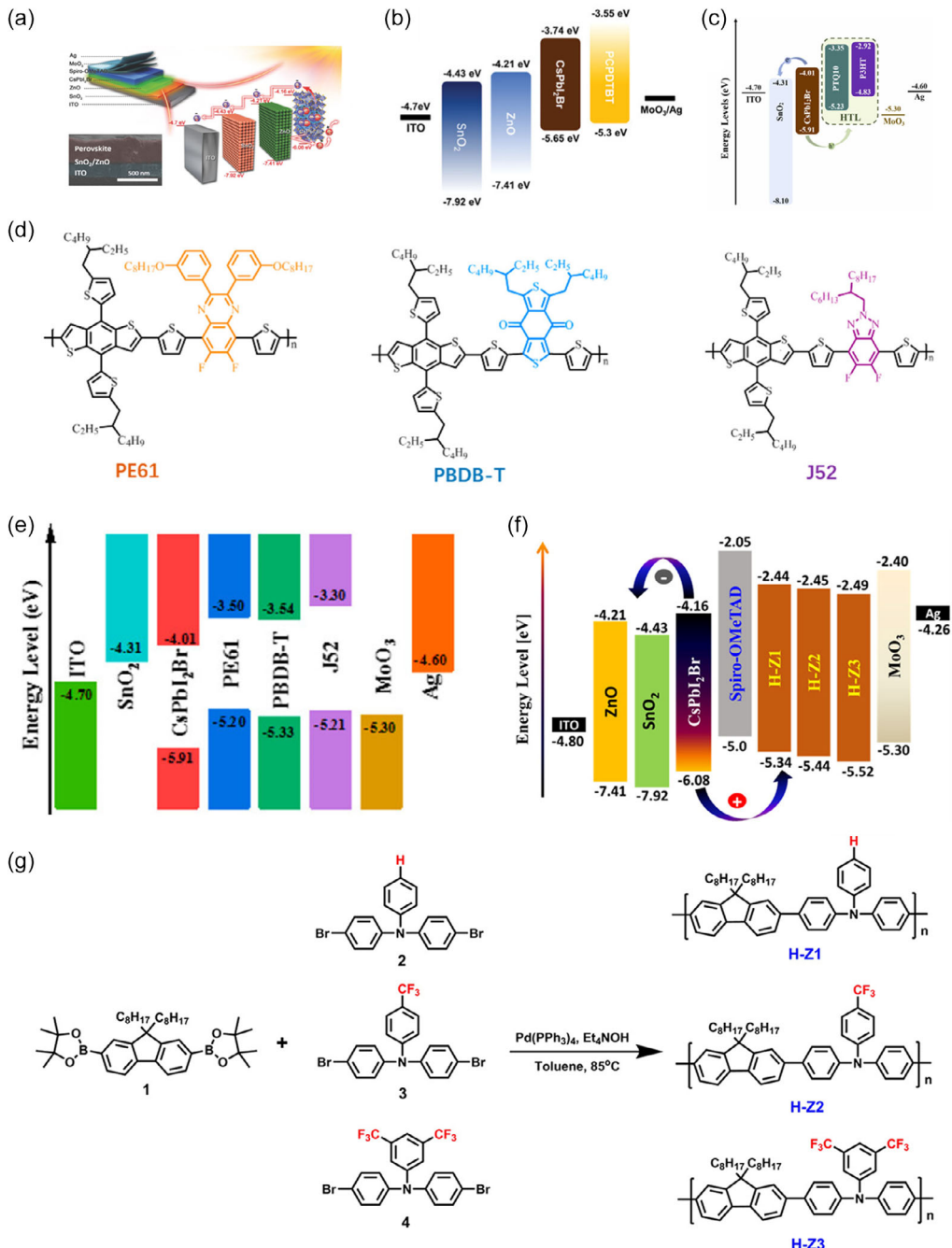


**Figure 7.** a) Device architecture of the all-inorganic  $\text{CsPbI}_2\text{Br}$  solar cells and the corresponding energy diagrams. Cross-section SEM image of the  $\text{CsPbI}_2\text{Br}$  perovskite film on  $\text{SnO}_2/\text{ZnO}$ . Reprinted with permission.<sup>[97]</sup> Copyright 2018, Wiley-VCH GmbH. b) Energy levels diagram of  $\text{CsPbI}_2\text{Br}$ -based PSCs. Reprinted with permission.<sup>[98]</sup> Copyright 2023, Wiley-VCH GmbH. c) Energy level diagram of  $\text{CsPbI}_2\text{Br}$ -based AIWPSCs with PTQ10 and P3HT as the HTL, respectively. Reprinted with permission.<sup>[99]</sup> Copyright 2022, Elsevier. d) Chemical structures of PE61, PBDB-T, and J52. Reprinted with permission.<sup>[100]</sup> Copyright 2023, American Chemical Society. e) Energy level diagram of AIWPSCs with different HTLs. Reprinted with permission.<sup>[100]</sup> Copyright 2023, American Chemical Society. f) Energy level diagram of AIWPSCs with Spiro-OMeTAD, H-Z1, H-Z2, and H-Z3 as the HTL, respectively. Reprinted with permission.<sup>[95]</sup> Copyright 2019, Wiley-VCH GmbH. g) The synthetic routes of H-Z1, H-Z2, and H-Z3.<sup>[95]</sup> Copyright 2019, Wiley-VCH GmbH.

PTQ10 and  $\text{CsPbI}_2\text{Br}$  than the classic P3HT (Figure 7c).<sup>[99]</sup> Moreover, the functional groups of PTQ10 can effectively passivate the surface defects of perovskite films. As a result, a device efficiency of 17.8% is obtained for the  $\text{CsPbI}_2\text{Br}$ -based

device. Dai et al. demonstrated that D- $\pi$ -A type polymers (PE61, PBDB-T, J52) (Figure 7d) can serve as dopant-free HTMs for AIWPSCs (Figure 7e).<sup>[100]</sup> The composition of the A unit plays a critical role in influencing the energy level, hole

mobility, and molecular stacking properties of these HTMs, consequently affecting the performance of AIWPSCs. Moreover, to minimize the energy loss caused by the energy difference at the perovskite/HTL interface, Yip et al. synthesized deep HOMO level HTMs (H-Z1, H-Z2, and H-Z3) to replace Spiro-OMeTAD (Figure 7f,g).<sup>[95]</sup> Benefited from the improved energy level alignment between the CsPbI<sub>2</sub>Br film and HTL, a champion device with a high  $V_{OC}$  of 1.3 V is achieved. Moreover, Chang et al. adopted HTL-free AIWPSCs. By optimizing the energy level through low concentration CsBr/CH<sub>3</sub>OH treatment and improving the hole transport ability, AIWPSCs with 9.48% efficiency and 1.54 V open voltage were prepared.<sup>[101]</sup>

Overall, the electrical properties of the ETL and HTL play a critical role in influencing the perovskite crystallization properties and charge transport properties of AIWPSCs. Although ZnO and SnO<sub>2</sub> have been investigated for their potential as ETLs in AIWPSCs, it is noted that significant energy losses still persist. Moreover, the undesirable energy level alignment between the perovskite films and HTLs also leads to seriously reduced device efficiency. Therefore, it is believed that with the development of high-performance CTMs with high charge mobility, excellent stability, suitable energy level, and excellent passivation ability, the device performance of AIWPSCs can be further improved.

## 5. Conclusion and Outlook

Although all-inorganic perovskite solar cells have made tremendous progress, specific issues still exist. Among which phase stability is one of the main concerns, especially for perovskite components modulated by mixed cations and halogen ions, phase stability is a key problem for device development and efficiency improvement, which is mainly due to the low tolerance coefficient and high defect density of all-inorganic perovskites. While chemical composition modulation, such as A-site, B-site, and X-site ions, has been employed to enhance  $\tau$  values and modulate crystallization properties of all-inorganic perovskites, the phase stability of all-inorganic perovskites remains a persistent challenge. Although other creative methods (solvent engineering, additive engineering) have also been designed to enhance phase stability and inhibit defect density, all-inorganic perovskites still suffer from compromised crystallization properties and high energy loss, which leads to confined device performance.

In contrast, interface defects can be considered as the main reasons for charge recombination at the interface. Suitable interface modification can significantly suppress the formation of defects on the surface of the perovskite film. In addition, interfacial recombination in all-inorganic perovskite devices can also be induced by the energy level mismatch between the perovskite film and CTls, which may cause charge accumulation and increase recombination. As a result, efforts have been made to explore HTMs and ETMs with better energy level matching.

In conclusion, the development of AIWPSCs, including phase stability, device performance progress, and device optimization strategies, is systematically elaborated. It is evident from our review that all-inorganic perovskites have not yet reached their full performance potential. Research in areas such as solvent engineering, additive engineering, interface modification, and the exploration of new CTMs is still necessary to achieve

high-performance AIWPSCs. We believe that there are two main directions for the improvement of device stability and device efficiency of AIWPSCs. On one hand, revealing the intrinsic crystallization kinetics of AIWPSCs is essential to guide the optimization strategies for enhancing the crystallization properties of all-inorganic perovskites. This includes but is not limited to identifying solvents with suitable precursor resolving capabilities, figuring out effective anti-solvents capable of modulating the initial crystallization process of AIWPSCs, synthesizing functional additives with outstanding defect passivation abilities, and exploring effective interface modification methods that can facilitate charge transfer from perovskite layers to the CTls. On the other hand, the structure of AIWPSCs needs to be further optimized. High-performance CTMs with energy levels aligned with those of the connected perovskite films and electrodes, coupled with effective passivation abilities to perovskite surface defects, are highly desired for the further enhancement of the AIWPSCs performance. Once efficiency and phase stability challenges are addressed, all-inorganic perovskites, characterized by their high thermal stability and suitable wide bandgap for the front sub-cell of tandem structures, have the potential to enhance the efficiency records of perovskite/organic, perovskite/perovskite, and perovskite/silicon TSCs, thereby advancing their commercialization.

## Acknowledgements

X.-Y.L. and Q.S. contributed equally to this work. The authors acknowledge financial support from the Science and Technology Development Fund, Macao SAR (0068/2022/A, 0006/2021/AKP, 0051/2021/A), Jiangsu Key Laboratory for Carbon-Based Functional Materials & Devices (ZZ2102), and Gusu Innovation and Entrepreneur Leading Talents (ZXL2023185). This work is also supported by the Suzhou Key Laboratory of Functional Nano & Soft Materials, the Collaborative Innovation Center of Suzhou Nano Science and Technology (NANO-CIC), the 111 Project, Joint International Research Laboratory of Carbon-Based Functional Materials and Devices, and Jiangsu Key Laboratory of Advanced Negative Carbon Technologies.

## Conflict of Interest

The authors declare no conflict of interest.

## Keywords

all-inorganic perovskite solar cells, charge transport layer, crystallization modification, phase stability, photovoltaic parameters

Received: November 15, 2023

Revised: January 2, 2024

Published online: January 26, 2024

- [1] T. Niu, Y. M. Xie, Q. Xue, S. Xun, Q. Yao, F. Zhen, W. Yan, H. Li, J. L. Brédas, H. L. Yip, *Adv. Energy Mater.* **2022**, *12*, 2102973.
- [2] S. Sajid, A. M. Elseman, H. Huang, J. Ji, S. Dou, H. Jiang, X. Liu, D. Wei, P. Cui, M. Li, *Nano Energy* **2018**, *51*, 408.
- [3] K. Wang, D. Yang, C. Wu, J. Shapter, S. Priya, *Joule* **2019**, *3*, 311.
- [4] Y. Hu, T. Niu, Y. Liu, Y. Zhou, Y. Xia, C. Ran, Z. Wu, L. Song, P. Müller-Buschbaum, Y. Chen, *ACS Energy Lett.* **2021**, *6*, 2917.

- [5] H. S. Jung, G. S. Han, N.-G. Park, M. J. Ko, *Joule* **2019**, *3*, 1850.
- [6] P. You, Z. Liu, Q. Tai, S. Liu, F. Yan, *Adv. Mater.* **2015**, *27*, 3632.
- [7] Q.-W. Liu, S. Yuan, S.-Q. Sun, W. Luo, Y.-J. Zhang, L.-S. Liao, M.-K. Fung, *J. Mater. Chem. C* **2019**, *7*, 4344.
- [8] S.-Q. Sun, X.-C. Hua, Q.-W. Liu, T.-T. Wang, W. Luo, Y.-J. Zhang, L.-S. Liao, M.-K. Fung, *J. Mater. Chem. C* **2019**, *7*, 2905.
- [9] D. Liu, Y. Li, J. Yuan, Q. Hong, G. Shi, D. Yuan, J. Wei, C. Huang, J. Tang, M.-K. Fung, *J. Mater. Chem. A* **2017**, *5*, 5701.
- [10] A. Kojima, K. Teshima, Y. Shirai, T. Miyasaka, *J. Am. Chem. Soc.* **2009**, *131*, 6050.
- [11] Y. Zhao, F. Ma, Z. Qu, S. Yu, T. Shen, H.-X. Deng, X. Chu, X. Peng, Y. Yuan, X. Zhang, *Science* **2022**, *377*, 531.
- [12] Y. M. Xie, Q. Yao, Q. Xue, Z. Zeng, T. Niu, Y. Zhou, M. P. Zhuo, S. W. Tsang, H. L. Yip, Y. Cao, *Interdiscip. Mater.* **2022**, *1*, 281.
- [13] Best Research-Cell Efficiency Chart, <https://www.nrel.gov/pv/cell-efficiency.html> (accessed: September 2023).
- [14] Z. Zeng, J. Zhang, X. Gan, H. Sun, M. Shang, D. Hou, C. Lu, R. Chen, Y. Zhu, L. Han, *Adv. Energy Mater.* **2018**, *8*, 1801050.
- [15] R. J. Sutton, G. E. Eperon, L. Miranda, E. S. Parrott, B. A. Kamino, J. B. Patel, M. T. Hörantner, M. B. Johnston, A. A. Haghighirad, D. T. Moore, H. J. Snaith, *Adv. Energy Mater.* **2016**, *6*, 1502458.
- [16] Y.-M. Xie, C. Ma, X. Xu, M. Li, Y. Ma, J. Wang, H. T. Chandran, C.-S. Lee, S.-W. Tsang, *Nano Res.* **2019**, *12*, 1033.
- [17] Y.-M. Xie, X. Xu, C. Ma, M. Li, Y. Ma, C.-S. Lee, S.-W. Tsang, *ACS Appl. Mater. Interfaces* **2019**, *11*, 25909.
- [18] T. Moot, A. R. Marshall, L. M. Wheeler, S. N. Habisreutinger, T. H. Schloemer, C. C. Boyd, D. R. Dikova, G. F. Pach, A. Hazarika, M. D. McGehee, H. J. Snaith, J. M. Luther, *Adv. Energy Mater.* **2020**, *10*, 1903365.
- [19] W. Chen, J. Zhang, G. Xu, R. Xue, Y. Li, Y. Zhou, J. Hou, Y. Li, *Adv. Mater.* **2018**, *30*, 1800855.
- [20] L. Liu, P. Liu, S. Ullah, S.-E. Yang, H. Guo, L. Wang, X. Wang, Y. Chen, *Solar Energy* **2021**, *228*, 274.
- [21] Z. Wang, L. Zeng, T. Zhu, H. Chen, B. Chen, D. J. Kubicki, A. Balvanz, C. Li, A. Maxwell, E. Ugur, et al., *Nature* **2023**, *618*, 74.
- [22] Q. Yao, Y. M. Xie, Y. Z. Zhou, Q. F. Xue, X. Xu, Y. J. Gao, T. Q. Niu, L. H. Chu, Z. S. Zhou, F. R. Lin, A. K. Y. Jen, T. T. Shi, H. L. Yip, Y. Cao, *Adv. Funct. Mater.* **2023**, *33*, 2212599.
- [23] S. Q. Sun, X. Xu, Q. Sun, Q. Yao, Y. Cai, X. Y. Li, Y. L. Xu, W. He, M. Zhu, X. Lv, F. R. Lin, A. K. Y. Jen, T. Shi, H. L. Yip, M. K. Fung, Y. M. Xie, *Adv. Energy Mater.* **2023**, *13*, 2204347.
- [24] Y. M. Xie, Z. Zeng, X. Xu, C. Ma, Y. Ma, M. Li, C. S. Lee, S. W. Tsang, *Small* **2020**, *16*, e1907226.
- [25] L. Tao, J. Qiu, B. Sun, X. Wang, X. Ran, L. Song, W. Shi, Q. Zhong, P. Li, H. Zhang, Y. Xia, P. Müller-Buschbaum, Y. Chen, *J. Energy Chem.* **2021**, *61*, 395.
- [26] R. Montecucco, E. Quadrivi, R. Po, G. Grancini, *Adv. Energy Mater.* **2021**, *11*, 2100672.
- [27] Y. Wei, Y. Zhao, C. Liu, Z. Wang, F. Jiang, Y. Liu, Q. Zhao, D. Yu, M. Hong, *Adv. Funct. Mater.* **2021**, *31*, 2106386.
- [28] K. Wang, C. Gao, Z. Xu, Q. Tian, X. Gu, L. Zhang, S. Zhang, K. Zhao, S. Liu, *Adv. Funct. Mater.* **2021**, *31*, 2101568.
- [29] X. Chu, Q. Ye, Z. Wang, C. Zhang, F. Ma, Z. Qu, Y. Zhao, Z. Yin, H.-X. Deng, X. Zhang, *Nat. Energy* **2023**, *8*, 372.
- [30] W. Xiang, Z. Wang, D. J. Kubicki, W. Tress, J. Luo, D. Prochowicz, S. Akin, L. Emsley, J. Zhou, G. Dietler, *Joule* **2019**, *3*, 205.
- [31] N. Li, Z. Zhu, J. Li, A. K. Y. Jen, L. Wang, *Adv. Energy Mater.* **2018**, *8*, 1800525.
- [32] Q. Chen, N. De Marco, B. Song, C.-C. Chen, H. Zhao, Z. Hong, H. Zhou, Y. Yang, *Nano Today* **2015**, *10*, 355.
- [33] W. Ahmad, J. Khan, G. Niu, J. Tang, *Solar RRL* **2017**, *1*, 1700048.
- [34] G. E. Eperon, G. M. Paternò, R. J. Sutton, A. Zampetti, A. A. Haghighirad, F. Cacialli, H. J. Snaith, *J. Mater. Chem. A* **2015**, *3*, 19688.
- [35] Q. Ma, S. Huang, S. Chen, M. Zhang, C. F. J. Lau, M. N. Lockrey, H. K. Mulmudi, Y. Shan, J. Yao, J. Zheng, *J. Phys. Chem. C* **2017**, *121*, 19642.
- [36] Y.-M. Xie, Q. Xue, H.-L. Yip, *Adv. Energy Mater.* **2021**, *11*, 2100784.
- [37] S.-Y. Yuan, H. Zhao, Y.-T. Wang, Z.-Z. Li, X.-D. Wang, W.-P. Cao, *J. Solid State Chem.* **2023**, *328*, 124299.
- [38] W. Xiang, S. Liu, W. Tress, *Energy Environ. Sci.* **2021**, *14*, 2090.
- [39] W. Xiang, W. Tress, *Adv. Mater.* **2019**, *31*, 1902851.
- [40] K. Yonezawa, K. Yamamoto, M. Shahiduzzaman, Y. Furumoto, K. Hamada, T. S. Ripples, M. Karakawa, T. Kuwabara, K. Takahashi, S. Hayase, T. Taima, *Jpn. J. Appl. Phys.* **2017**, *56*, 04cs11.
- [41] S. Tan, B. Yu, Y. Cui, F. Meng, C. Huang, Y. Li, Z. Chen, H. Wu, J. Shi, Y. Luo, D. Li, Q. Meng, *Angew. Chem. Int. Ed.* **2022**, *61*, e202201300.
- [42] Y. Chen, X. Wang, Y. Wang, X. Liu, Y. Miao, Y. Zhao, *Sci. Bull.* **2023**, *68*, 706.
- [43] J. A. Steele, H. Jin, I. Dovgaliku, R. F. Berger, T. Braeckeveldt, H. Yuan, C. Martin, E. Solano, K. Lejaeghere, S. M. Rogge, *Science* **2019**, *365*, 679.
- [44] P. Wang, X. Zhang, Y. Zhou, Q. Jiang, Q. Ye, Z. Chu, X. Li, X. Yang, Z. Yin, J. You, *Nat. Commun.* **2018**, *9*, 2225.
- [45] Y. Wang, X. Liu, T. Zhang, X. Wang, M. Kan, J. Shi, Y. Zhao, *Angew. Chem. Int. Ed.* **2019**, *58*, 16691.
- [46] X. Chang, J. Fang, Y. Fan, T. Luo, H. Su, Y. Zhang, J. Lu, L. Tsetseris, T. D. Anthopoulos, S. F. Liu, K. Zhao, *Adv. Mater.* **2020**, *32*, e2001243.
- [47] S. Tan, J. Shi, B. Yu, W. Zhao, Y. Li, Y. Li, H. Wu, Y. Luo, D. Li, Q. Meng, *Adv. Funct. Mater.* **2021**, *31*, 2010813.
- [48] J. Liang, C. Wang, Y. Wang, Z. Xu, Z. Lu, Y. Ma, H. Zhu, Y. Hu, C. Xiao, X. Yi, *J. Am. Chem. Soc.* **2016**, *138*, 15829.
- [49] M. Cheng, C. Chen, K. Aitola, F. Zhang, Y. Hua, G. Boschloo, L. Kloof, L. Sun, *Chem. Mater.* **2016**, *28*, 8631.
- [50] X. Zheng, B. Chen, J. Dai, Y. Fang, Y. Bai, Y. Lin, H. Wei, X. C. Zeng, J. Huang, *Nat. Energy* **2017**, *2*, 17102.
- [51] Y. Zhao, J. Zhu, B. He, Q. Tang, *ACS Appl. Mater. Interfaces* **2021**, *13*, 11058.
- [52] J. Zhu, B. He, W. Zhang, R. Tui, H. Chen, Y. Duan, H. Huang, J. Duan, Q. Tang, *Adv. Funct. Mater.* **2022**, *32*, 2206838.
- [53] J. Dou, J. Tan, B. He, J. Duan, Q. Tang, *Dalton Trans.* **2023**, *52*, 6146.
- [54] X. Fu, K. Zhou, Y. Min, Y. Qian, J. Mater. Sci.: Mater. Electron. **2022**, *33*, 17649.
- [55] S. S. Mali, J. V. Patil, P. S. Shinde, G. de Miguel, C. K. Hong, *Matter* **2021**, *4*, 635.
- [56] J. Sun, Y. Jin, Q. Liu, F. Qiu, *Chem. Eng. J.* **2023**, *457*, 141300.
- [57] F. Yu, J. Liu, P. Xu, J. Huang, C.-H. Li, Y.-X. Zheng, *J. Solid State Chem.* **2023**, *317*, 123728.
- [58] S. Zheng, H. Wang, J. Li, P. Wei, Y. Qi, Y. Xie, *Opt. Mater.* **2023**, *136*, 113427.
- [59] C. Liu, W. Li, C. Zhang, Y. Ma, J. Fan, Y. Mai, *J. Am. Chem. Soc.* **2018**, *140*, 3825.
- [60] T. Leijtens, K. Bush, R. Cheacharoen, R. Beal, A. Bowring, M. D. McGehee, *J. Mater. Chem. A* **2017**, *5*, 11483.
- [61] X. Jia, C. Zuo, S. Tao, K. Sun, Y. Zhao, S. Yang, M. Cheng, M. Wang, Y. Yuan, J. Yang, *Sci. Bull.* **2019**, *64*, 1532.
- [62] S. Chen, T. Zhang, X. Liu, J. Qiao, L. Peng, J. Wang, Y. Liu, T. Yang, J. Lin, *J. Mater. Chem. C* **2020**, *8*, 3351.
- [63] Z. Wang, A. K. Baranwal, M. A. Kamarudin, Y. Kamata, C. H. Ng, M. Pandey, T. Ma, S. Hayase, *J. Mater. Chem. A* **2019**, *7*, 20390.
- [64] Z. Guo, S. Zhao, A. Liu, Y. Kamata, S. Teo, S. Yang, Z. Xu, S. Hayase, T. Ma, *ACS Appl. Mater. Interfaces* **2019**, *11*, 19994.

- [65] C. F. J. Lau, Z. Wang, N. Sakai, J. Zheng, C. H. Liao, M. Green, S. Huang, H. J. Snaith, A. Ho-Baillie, *Adv. Energy Mater.* **2019**, 9, 1901685.
- [66] L. Duan, H. Zhang, M. Liu, M. Grätzel, J. Luo, *ACS Energy Lett.* **2022**, 7, 2911.
- [67] Y. Che, Z. Liu, Y. Duan, J. Wang, S. Yang, D. Xu, W. Xiang, T. Wang, N. Yuan, J. Ding, S. F. Liu, *Angew. Chem. Int. Ed.* **2022**, 61, e202205012.
- [68] R. Montecucco, G. Pica, V. Romano, F. De Boni, S. Cavalli, G. Bruni, E. Quadrivi, M. De Bastiani, M. Prato, R. Po, G. Grancini, *Solar RRL* **2023**, 7, 2300358.
- [69] C. Liu, W. Li, H. Li, H. Wang, C. Zhang, Y. Yang, X. Gao, Q. Xue, H.-L. Yip, J. Fan, R. E. I. Schropp, Y. Mai, *Adv. Energy Mater.* **2019**, 9, 1803572.
- [70] U.-G. Jong, C.-J. Yu, Y.-H. Kye, Y.-S. Kim, C.-H. Kim, S.-G. Ri, *J. Mater. Chem. A* **2018**, 6, 17994.
- [71] J. K. Nam, S. U. Chai, W. Cha, Y. J. Choi, W. Kim, M. S. Jung, J. Kwon, D. Kim, J. H. Park, *Nano Lett.* **2017**, 17, 2028.
- [72] T. Ozturk, E. Akman, A. E. Shalan, S. Akin, *Nano Energy* **2021**, 87, 106157.
- [73] J. Ma, M. Qin, Y. Li, T. Zhang, J. Xu, G. Fang, X. Lu, *J. Mater. Chem. A* **2019**, 7, 27640.
- [74] J. Song, H. Xie, E. L. Lim, Y. Li, T. Kong, Y. Zhang, X. Zhou, C. Duan, D. Bi, *Solar RRL* **2022**, 6, 2100880.
- [75] J. He, J. Su, Z. Lin, J. Ma, L. Zhou, S. Zhang, S. Liu, J. Chang, Y. Hao, *Adv. Sci.* **2021**, 8, 2101367.
- [76] J. Bahadur, J. Ryu, P. Pandey, S. Cho, J. S. Cho, D. W. Kang, *Nanoscale* **2023**, 15, 3850.
- [77] S. Liu, X. Xu, C. Xing, G. Ge, D. Wang, T. Zhang, *Energy Technol.* **2022**, 10, 2200378.
- [78] S. Zhang, S. Wu, W. Chen, H. Zhu, Z. Xiong, Z. Yang, C. Chen, R. Chen, L. Han, W. Chen, *Mater. Today Energy* **2018**, 8, 125.
- [79] H. Zai, D. Zhang, L. Li, C. Zhu, S. Ma, Y. Zhao, Z. Zhao, C. Chen, H. Zhou, Y. Li, Q. Chen, *J. Mater. Chem. A* **2018**, 6, 23602.
- [80] X. Wang, X. Ran, X. Liu, H. Gu, S. Zuo, W. Hui, H. Lu, B. Sun, X. Gao, J. Zhang, Y. Xia, Y. Chen, W. Huang, *Angew. Chem. Int. Ed.* **2020**, 59, 13354.
- [81] Y. Lv, Y. Li, Y. Zhou, J. Liu, J. Wang, Y. Lin, J. Hu, T. Pan, Y. Li, K. Wang, Y. Xia, W. Shi, Y. Chen, *ACS Appl. Mater. Interfaces* **2023**, 15, 29236.
- [82] X. Ding, Y. Zhang, F. Sheng, Y. Li, L. Zhi, X. Cao, X. Cui, D. Zhuang, J. Wei, *ACS Appl. Energy Mater.* **2021**, 4, 5504.
- [83] X. Sun, Z. Shao, Y. Rao, H. Meng, C. Gao, C. Chen, D. Liu, P. Lv, Z. Li, X. Wang, G. Cui, S. Pang, *Adv. Energy Mater.* **2020**, 11, 2002754.
- [84] C. Dong, X. Han, W. Li, Q. Qiu, J. Wang, *Nano Energy* **2019**, 59, 553.
- [85] J. Yang, H. Yu, S. Wu, C. Cai, J. Gao, X. Lu, X. Gao, L. Shui, S. Wu, J.-M. Liu, *ACS Appl. Energy Mater.* **2022**, 5, 2881.
- [86] X. Huo, W. Sun, K. Wang, W. Liu, R. Yin, Y. Sun, Y. Gao, T. You, P. Yin, *ACS Appl. Mater. Interfaces* **2023**, 15, 9382.
- [87] J. He, J. Su, J. Di, Z. Lin, S. Zhang, J. Ma, J. Zhang, S. Liu, J. Chang, Y. Hao, *Nano Energy* **2022**, 94, 106960.
- [88] J. He, Q. Wang, Y. Xu, X. Guo, L. Zhou, J. Su, Z. Lin, J. Zhang, Y. Hao, J. Chang, *Small* **2023**, 19, 2205962.
- [89] Q. Zeng, X. Zhang, X. Feng, S. Lu, Z. Chen, X. Yong, S. A. Redfern, H. Wei, H. Wang, H. Shen, *Adv. Mater.* **2018**, 30, 1705393.
- [90] X. Gu, W. Xiang, Q. Tian, S. F. Liu, *Angew. Chem. Int. Ed.* **2021**, 60, 23164.
- [91] J. Wang, J. Zhang, Y. Zhou, H. Liu, Q. Xue, X. Li, C. C. Chueh, H. L. Yip, Z. Zhu, A. K. Y. Jen, *Nat. Commun.* **2020**, 11, 177.
- [92] C. Kang, S. Xu, H. Rao, Z. Pan, X. Zhong, *ACS Energy Lett.* **2023**, 8, 909.
- [93] X. Fu, K. Zhou, X. Zhou, H. Ji, Y. Min, Y. Qian, *J. Solid State Chem.* **2022**, 308, 122891.
- [94] W. Zhu, W. Chai, D. Chen, J. Ma, D. Chen, H. Xi, J. Zhang, C. Zhang, Y. Hao, *ACS Energy Lett.* **2021**, 6, 1500.
- [95] B. Zhang, Y. Zhou, Q. Xue, J. Tian, Q. Yao, Y. Zang, L. Wang, W. Yang, H.-L. Yip, Y. Cao, *Solar RRL* **2019**, 3, 1900265.
- [96] J. Ma, J. Su, Z. Lin, L. Zhou, J. He, J. Zhang, S. Liu, J. Chang, Y. Hao, *Nano Energy* **2020**, 67, 104241.
- [97] L. Yan, Q. Xue, M. Liu, Z. Zhu, J. Tian, Z. Li, Z. Chen, Z. Chen, H. Yan, H. L. Yip, Y. Cao, *Adv. Mater.* **2018**, 30, e1802509.
- [98] Z. W. Li, J. L. Wang, Y. Y. Deng, J. N. Xi, Y. Zhang, C. Y. Liu, W. B. Guo, *Adv. Funct. Mater.* **2023**, 33, 2214562.
- [99] Y. Ding, Q. Guo, Y. Geng, Z. Dai, Z. Wang, Z. Chen, Q. Guo, Z. Zheng, Y. Li, E. Zhou, *Nano Today* **2022**, 46, 101586.
- [100] Z. Dai, Q. Guo, Y. Ding, Z. Wang, N. Jiang, E. Zhou, *ACS Appl. Mater. Interfaces* **2023**, 15, 9784.
- [101] S. Zhang, J. He, X. Guo, J. Su, Z. Lin, J. Zhang, L. Guo, Y. Hao, J. Chang, *ACS Mater. Lett.* **2023**, 5, 1497.
- [102] X. Chang, W. Li, L. Zhu, H. Liu, H. Geng, S. Xiang, J. Liu, H. Chen, *ACS Appl. Mater. Interfaces* **2016**, 8, 33649.
- [103] J. Duan, Y. Zhao, X. Yang, Y. Wang, B. He, Q. Tang, *Adv. Energy Mater.* **2018**, 8, 1802346.
- [104] R. Guo, J. Xia, H. Gu, X. Chu, Y. Zhao, X. Meng, Z. Wu, J. Li, Y. Duan, Z. Li, Z. Wen, S. Chen, Y. Cai, C. Liang, Y. Shen, G. Xing, W. Zhang, G. Shao, *J. Mater. Chem. A* **2023**, 11, 408.
- [105] J. B. Hoffman, G. Zaiats, I. Wappes, P. V. Kamat, *Chem. Mater.* **2017**, 29, 9767.
- [106] X. Li, Y. Tan, H. Lai, S. Li, Y. Chen, S. Li, P. Xu, J. Yang, *ACS Appl. Mater. Interfaces* **2019**, 11, 29746.
- [107] Q. Zhou, J. Duan, J. Du, Q. Guo, Q. Zhang, X. Yang, Y. Duan, Q. Tang, *Adv. Sci.* **2021**, 8, e2101418.
- [108] J. Zhu, M. Tang, B. He, W. Zhang, X. Li, Z. Gong, H. Chen, Y. Duan, Q. Tang, *J. Mater. Chem. A* **2020**, 8, 20987.
- [109] Q. Tian, G. Ding, Y. Cai, Z. Li, X. Tang, R.-J. Xie, P. Gao, *ACS Appl. Energy Mater.* **2021**, 4, 7535.
- [110] Q. Guo, Z. Dai, C. Dong, Y. Ding, N. Jiang, Z. Wang, L. Gao, C. Duan, Q. Guo, E. Zhou, *Chem. Eng. J.* **2023**, 461, 142025.
- [111] Z. Guo, A. K. Jena, I. Takei, M. Ikegami, A. Ishii, Y. Numata, N. Shibayama, T. Miyasaka, *Adv. Funct. Mater.* **2021**, 31, 2103614.
- [112] J. V. Patil, S. S. Mali, C. K. Hong, *Solar RRL* **2020**, 4, 2000164.
- [113] E. C. Shen, J. D. Chen, Y. Tian, Y. X. Luo, Y. Shen, Q. Sun, T. Y. Jin, G. Z. Shi, Y. Q. Li, J. X. Tang, *Adv. Sci.* **2020**, 7, 1901952.
- [114] Y. Wang, T. Zhang, F. Xu, Y. Li, Y. Zhao, *Solar RRL* **2018**, 2, 1700180.
- [115] H. Xiao, C. Zuo, L. Zhang, W. Zhang, F. Hao, C. Yi, F. Liu, H. Jin, L. Ding, *Nano Energy* **2023**, 106, 108061.
- [116] G. Yin, H. Zhao, H. Jiang, S. Yuan, T. Niu, K. Zhao, Z. Liu, S. F. Liu, *Adv. Funct. Mater.* **2018**, 28, 1803269.
- [117] W. Chen, D. Li, S. Chen, S. Liu, Y. Shen, G. Zeng, X. Zhu, E. Zhou, L. Jiang, Y. Li, Y. Li, *Adv. Energy Mater.* **2020**, 10, 2000851.
- [118] C. F. J. Lau, X. Deng, Q. Ma, J. Zheng, J. S. Yun, M. A. Green, S. Huang, A. W. Y. Ho-Baillie, *ACS Energy Lett.* **2016**, 1, 573.
- [119] W. Li, M. U. Rothmann, A. Liu, Z. Wang, Y. Zhang, A. R. Pascoe, J. Lu, L. Jiang, Y. Chen, F. Huang, Y. Peng, Q. Bao, J. Etheridge, U. Bach, Y. B. Cheng, *Adv. Energy Mater.* **2017**, 7, 1700946.
- [120] Q. Liu, J. Qiu, X. Yan, Y. Fei, Y. Qiang, Q. Chang, Y. Wei, X. Zhang, W. Tian, S. Jin, Z. Yu, L. Sun, *J. Energy Chem.* **2022**, 74, 387.
- [121] J. Wang, X. Wu, Y. Liu, Q. Xue, H.-L. Yip, A. K. Y. Jen, Z. Zhu, *Energy Technol.* **2021**, 9, 2100562.
- [122] B. Xu, D. Liu, C. Dong, M. Awais, W. Wang, Y. Song, Y. Deng, M. Yao, J. Tong, G. Yue, W. Zhang, F. Tan, M. I. Saidaminov, *J. Colloid Interface Sci.* **2023**, 641, 105.
- [123] W. Zhu, W. Chai, M. Deng, D. Chen, D. Chen, J. Zhang, C. Zhang, Y. Hao, *Electrochim. Acta* **2020**, 330, 135325.
- [124] W. Zhu, Q. Zhang, D. Chen, Z. Zhang, Z. Lin, J. Chang, J. Zhang, C. Zhang, Y. Hao, *Adv. Energy Mater.* **2018**, 8, 1802080.



**Xin-Yi Li** received her B.S. degree (2022) from the College of Science of Jiangsu Ocean University. Now, she is a graduate student at the Institute of Function Nano & Soft Materials (FUNSOM) of Soochow University under the supervision of Professor Roy Man-Keung Fung and Dr. Yue-Min Xie. Her research mainly focuses on defect and interface engineering for high-efficiency perovskite-based TSCs.



**Qi Sun** received her Master degree in physics from Soochow University in 2017 and joined the Institute of Functional Nano & Soft Materials (FUNSOM), Soochow University as a technician in 2018. Now, she is a Ph.D. student at Macao Institute of Materials Science and Engineering (MIMSE), Macau University of Science and Technology. Her research mainly focuses on high-efficiency white-color organic-light-emitting diodes (OLEDs), perovskite LEDs and solar cells.



**Yue-Min Xie** is an associate professor at the Institute of Functional Nano & Soft Materials (FUNSOM) of Soochow University. Before joining FUNSOM, he was a postdoctoral researcher in the State Key Laboratory of Luminescent Materials and Devices at South China University of Technology from 2020–2022. He received his Master's degree (2016) at FUNSOM, and completed his Ph.D. degree (2019) in MSE from City University of Hong Kong (CityU). His research mainly focuses on the crystallization kinetics and device engineering for perovskite optoelectronic devices, perovskite-based tandem devices, and OLEDs.



**Man-Keung Fung** received his Ph.D. degree in materials science from the City University of Hong Kong. Now, he is a professor of the Institute of Functional Nano & Soft Materials (FUNSOM), Soochow University, and Macao Institute of Materials Science and Engineering (MIMSE). He has over 20 years of fundamental and applied research experience in organic light-emitting diode (OLED) displays and lighting, flexible OLEDs, and thin-film encapsulation technology. His research mainly focuses on white-color OLEDs for AMOLED, lighting, and micro-displays, flexible OLEDs and their thin film encapsulation, perovskite LEDs and solar cells, semiconductor surfaces and interfaces.